DOI: 10.1002/chem.201302181

Nearly Degenerate Isomers of $C(BH)_2$: Cumulene, Carbene, or Carbone?

Shiblee R. Barua,[a] Wesley D. Allen,*[a] Elfi Kraka,*[b] Paul Jerabek,[c] Rebecca Sure,[c] and Gernot Frenking*[c]

Abstract: The ground electronic state of $C(BH)_2$ exhibits both a linear minimum and a peculiar angle-deformation isomer with a central B-C-B angle near 90°. Definitive computations on these species and the intervening transition state have been executed by means of coupled-cluster theory including single and double excitations (CCSD), perturbative triples (CCSD(T)), and full triples with perturbative quadruples (CCSDT(Q)), in concert with series of correlation-consistent basis sets (cc-pV*X*Z, *X* = D, T, Q, 5, 6; cc-pCV*X*Z, *X* = T, Q). Final energies were pinpointed by focal-point analyses (FPA) targeting the complete basis-set limit of CCSDT(Q) theory with auxiliary core correlation, relativistic, and non-Born–Oppenheimer corrections. Isomerization of the linear species to the bent form has a minuscule FPA reaction energy of 0.02 kcal mol^{-1} and a corresponding barrier of only 1.89 kcal mol^{-1}. Quantum tunneling computations reveal interconversion of the two isomers on a timescale much less than 1 s even at 0 K. Highly accurate CCSD(T)/cc-pVTZ and composite c~CCSDT(Q)/cc-pCVQZ anharmonic vibrational frequencies confirm matrix-isolation infrared bands previously assigned to linear $C(BH)_2$ and provide excellent predictions for the heretofore unobserved bent isomer. Chemical bonding in the $C(BH)_2$ species was exhaustively investigated by the atoms-in-molecules (AIM) approach, molecular orbital plots, various population analyses, local mode vibrations and force constants, unified reaction valley analysis (URVA), and other methods. Linear $C(BH)_2$ is a cumulene, whereas bent $C(BH)_2$ is best characterized as a carbene with little carbone character. Weak B–B attraction is clearly present in the unusual bent isomer, but its strength is insufficient to form a CB_2 ring with a genuine boron–boron bond and attendant AIM bond path.

Keywords: bond energy · carbenes · carbones · cumulenes · density functional calculations

Introduction

Recent theoretical[1] and experimental[2] studies have revealed a class of divalent carbon(0) compounds CL_2 that exhibit peculiar bonding and chemical reactivity clearly distinguishable from carbenes CR_2. These compounds have been designated as carbones and may be viewed as donor–acceptor complexes L→C←L between a bare carbon atom in the excited ^1D state and two σ-donor ligands L. In contrast, carbenes involve two electron-sharing bonds between the substituents R and a ground-state ^3P carbon atom.[1] Stable carbones, which typically have L-C-L bending angles near 130°, have been synthesized with L = phosphine (carbodiphosphoranes, $C(PR_3)_2$)[3] and L = carbene (carbodicarbenes, $C(CR_2)_2$).[2a–f] Carbon suboxide (C_3O_2), which is usually rendered with cumulated double bonds (O=C=C=C=O),[4] has also been considered a OC→C←CO donor–acceptor species.[1c–g] The carbone bonding model nicely explains why C_3O_2 has a bent gas-phase equilibrium geometry with ∢(C-C-C) = 156°,[5] the larger bending angle relative to carbodiphosphoranes and carbodicarbenes coming from the higher π-acceptor strength of CO.[6]

Theoretical searches for synthetically viable carbones have found that carbodiylides $C(ECp^*)_2$ (E = Al to Tl; Cp* = pentamethylcyclopentadienyl) are strongly bonded molecules with E-C-E bending angles of 100–105°.[7] In contrast to the heavier group 13 homologues, $C(BCp^*)_2$ was computed to have a linear B-C-B arrangement. This finding was explained in terms of a Cp*B=C=BCp* structure with electron-sharing bonds and boron in the formal oxidation state III, at variance with the carbodiylides $C(ECp^*)_2$ (E = Al to Tl) that possess donor–acceptor bonds Cp*E→C←ECp* with the elements E in oxidation state I.

The theoretical studies of $C(ECp^*)_2$ were investigated for the parent systems $C(EH)_2$.[8] The heavier homologues of

[a] S. R. Barua, Prof. W. D. Allen
Department of Chemistry and Center for Computational Chemistry
University of Georgia, Athens, Georgia 30602 (USA)
Fax: (+1) 706 542 0406
E-mail: wdallen@uga.edu

[b] Prof. E. Kraka
Department of Chemistry
Southern Methodist University, Dallas, Texas (USA)
Fax: (+1) 214 768 4089
E-mail: ekraka@smu.edu

[c] P. Jerabek, R. Sure, Prof. G. Frenking
Fachbereich Chemie, Philipps-Universität Marburg
Hans-Meerwein-Strasse 1, 35032 Marburg (Germany)
Fax: (+49) 6421285566
E-mail: frenking@chemie.uni-marburg.de

Supporting information for this article is available on the WWW under http://dx.doi.org/10.1002/chem.201302181.

$C(EH)_2$ with E = Al to Tl display equilibrium structures similar to $C(ECp^*)_2$ with $\sphericalangle$(E-C-E) = 100–110°. Thus, the electronic structure of $C(ER)_2$ for E = Al to Tl is mainly determined by the donor–acceptor interactions RE→C←ER, and the substituents R play only a minor (steric) role in the equilibrium geometry. However, a peculiar result was found for the boron homologue $C(BH)_2$.[8] Geometry optimizations of the linear form gave an HB=C=BH equilibrium structure, but computations starting from a bent geometry yielded a second energy minimum with a very acute bending angle near 90°. A key question is whether the latter isomer might be considered a carbone HB→C←BH rather than a carbene. A striking result of the computations was the near energetic equivalence of the linear and bent isomers of $C(BH)_2$.[8]

In this work, we report cutting-edge computations of the intriguing potential-energy surface of $C(BH)_2$. We analyze the bonding in the linear (**1a**) and bent (**1b**) isomers as well as the intervening reaction path, while making comparisons to several reference molecules (Scheme 1). Furthermore, we

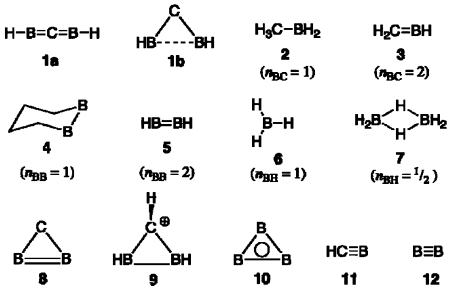

Scheme 1. Linear (**1a**) and bent (**1b**) isomers of $C(BH)_2$ along with relevant reference molecules.

pinpoint the energetic profile of the **1a**→**1b** isomerization and predict highly accurate vibrational spectra of the energy minima to aid future experimental work. A linear $C(BH)_2$ species was synthesized and spectroscopically identified in a low-temperature matrix by Hassanzadeh and Andrews in 1992.[9] Low-level quantum chemical computations (RHF/DZP) of the equilibrium geometry, vibrational frequencies, and infrared intensities were compared with experimental spectra to identify the molecule. However, only the linear HB=C=BH species was reported, and no assignments were made to the unconventional bent isomer. The present work reinvestigates the earlier findings in light of new, definitive computations on both isomers.

Computational Methods

High-level ab initio computations are crucial to accurately characterizing the nearly isoenergetic structural isomers of $C(BH)_2$. Equilibrium geometries and harmonic vibrational frequencies of the bent and linear isomers as well as the interconnecting transition state were determined using coupled-cluster theory[10] including full single and double excitations and a perturbative treatment of connected triple excitations (CCSD(T)).[11] Restricted Hartree–Fock reference wave functions were always employed. The computations were executed using the correlation-consistent polarized valence basis sets of the form cc-pV*X*Z (*X* = D, T, Q) and the associated core-valence cc-pCV*X*Z (*X* = T, Q) sets developed by Dunning and co-workers.[12]

The focal-point analysis (FPA) scheme of Allen and co-workers[13] was used to pinpoint relative energies by computing a hierarchical series of single-point energies at the CCSD(T)/cc-pVQZ reference geometries. Complete basis set (CBS) limits were found by extrapolating cc-pV(Q,5,6)Z Hartree–Fock[14] energies (E_{RHF}) and cc-pV(5,6)Z electron correlation energies (E_{corr}) by means of the functional forms[15] shown in Equations (1) and (2):

$$E_{RHF}(X) = E_{RHF}^{CBS} + ae^{-bX} \quad (1)$$

$$E_{corr}(X) = E_{corr}^{CBS} + bX^{-3} \quad (2)$$

Total energies at the CBS limit for second-order Møller–Plesset perturbation (MP2) theory,[16] the coupled-cluster singles and doubles (CCSD)[17] method, and CCSD(T)[11] theory were obtained by adding separate E_{RHF}^{CBS} and E_{corr}^{CBS} results from Equations (1) and (2). Our final coupled-cluster electron correlation energies included full treatments of singles, doubles, and triples and a perturbative accounting of quadruple excitations (CCSDT(Q)).[18] The following composite (c~) approximation [Eq. (3)] was used to extract CCSDT(Q) results for the CBS limit:[19]

$$E_{c\sim CCSDT(Q)}^{CBS} = E_{CCSD(T)}^{CBS} + E_{CCSDT(Q)}^{cc-pVTZ} - E_{CCSD(T)}^{cc-pVTZ} \quad (3)$$

The effects of the core electron correlation (Δ(core)), including the small shifts engendered in geometric structures, were evaluated with the cc-pCVQZ basis set[12b] by differencing all-electron (AE) CCSD(T)/cc-pCVQZ//AE-CCSD(T)/cc-pCVQZ and frozen-core (FC) CCSD(T)/cc-pCVQZ//FC-CCSD(T)/cc-pVQZ energies, in which // denotes "at the optimum geometry of". The diagonal Born–Oppenheimer correction (Δ(DBOC)) was included at the RHF/cc-pVQZ level. A first-order relativistic correction (Δ(rel)) from the one-electron mass-velocity and Darwin terms was also incorporated from FC-CCSD(T)/cc-pVQZ computations. In total, the final FPA relative energies were computed as shown in Equation (4) in which the zero-point vibrational energy (ZPVE) term was evaluated with FC-CCSD(T)/cc-pVQZ harmonic frequencies.

$$\Delta E(FPA) = E_{c\sim CCSDT(Q)}^{CBS} + \Delta(ZPVE) + \Delta(rel) + \Delta(DBOC) \quad (4)$$

The CCSD(T) geometry optimizations and harmonic vibrational frequency computations were performed using analytic gradient methods within the Mainz–Austin–Budapest (MAB) version of the ACESII program[20] or the successor CFOUR package.[21] The MP2, CCSD, and CCSD(T) single-point computations for the focal-point analyses were performed with the MOLPRO program.[22] The CCSDT(Q) results were obtained with the string-based MRCC code of Kállay using integrals generated from MAB ACESII;[18b,23] MRCC is a stand-alone program capable of performing arbitrary-order coupled-cluster and configuration-interaction energy computations.

Anharmonic vibrational frequencies were computed by application of second-order vibrational perturbation theory (VPT2)[24–27] to FC-CCSD(T)/cc-pVTZ and c~CCSDT(Q)/cc-pCVQZ complete internal-coordinate quartic force fields, as obtained by the INTDIF numerical differentiation program[28] from an optimal grid of tightly converged (10^{-12} E_h) energy points. The c~CCSDT(Q)/cc-pCVQZ force field was determined using the composite energy formula shown in Equation (5) and geometries were re-optimized at this level of theory before executing the numerical differentiation.

$$E_{c\sim CCSDT(Q)}^{cc\text{-}pCVQZ} = E_{AE-CCSD(T)}^{cc-pCVQZ} + E_{CCSDT(Q)}^{cc-pVDZ} - E_{CCSDT(T)}^{cc-pVDZ} \quad (5)$$

By enforcing strict $D_{\infty h}$ cylindrical symmetry[29] for **1a** and utilizing C_{2v} symmetry for **1b**, the full quartic force fields were accurately computed from only 239 and 568 points, respectively. The curvilinear force field transformations[30,31] from internal to normal coordinates were executed with the INTDER program,[32,33] after which vibrational anharmonicities

and spectroscopic constants were extracted with ANHARM.[33] A Fermi resonance threshold of 25 cm^{-1} was chosen for the VPT2 treatment.

Diagnostics of multireference character were applied to the ground electronic state of the $C(BH)_2$ stationary points. At the FC-CCSD/cc-pVQZ level of theory, the linear, bent, and transition-state structures displayed T_1 diagnostics[34] of 0.018, 0.016, and 0.017 and D_1 diagnostics[35] of 0.042, 0.038, and 0.038, respectively, all of which are smaller than the recommended multireference thresholds of 0.02 (T_1) and 0.05 (D_1). Moreover, the linear, bent, and transition-state maximum absolute t_2 amplitudes were only 0.066, 0.080, and 0.060 at the same level of theory. Finally, full-valence CASSCF/cc-pVQZ wave functions[36] (12 electrons in 14 molecular orbitals) were computed with MOLPRO to ascertain the leading configuration-interaction (CI) coefficients (C_1, C_2) for determinants constructed from CASSCF natural orbitals. The linear, bent, and transition-state structures exhibited $C_1 =$ 0.938, 0.938, and 0.940 and $C_2 =$ −0.100, −0.135, and −0.098, respectively, which revealed a clear dominance of the ground-state Hartree–Fock configuration. In summary, $C(BH)_2$ is predominantly a closed-shell system without substantial diradical character that can be accurately treated by the high-order single-reference coupled-cluster methods employed here. This conclusion is particularly germane for the unusual bent isomer.

Table 1. Linear $C(BH)_2$ isomer: optimized bond lengths (r_e, Å) and relative energies (ΔE_0, kcal mol^{-1}).[a]

	r_e(B−C)	r_e(B−H)	ΔE_0(bent−linear)	ΔE_0(TS−linear)	r_e(BH($^1\Sigma^+$))[b]
CCSD(T)					
cc-pVDZ	1.3801	1.1870	−0.161	+1.889	1.2558
cc-pVTZ	1.3648	1.1726	+0.057	+1.910	1.2354
cc-pVQZ	1.3616	1.1714	−0.114	+1.775	1.2333
cc-pCVTZ (AE)	1.3613	1.1712	+0.036	+1.904	1.2332
cc-pCVQZ (AE)	1.3578	1.1692	−0.127	+1.805	1.2302
c~CCSDT(Q)					
cc-pCVQZ(AE)	1.3587	1.1693	+0.191	–	1.2302

[a] All-electron, core-correlated results denoted by (AE); frozen-core otherwise. The ΔE_0 values include zero-point vibrational corrections. [b] Bond lengths of diatomic BH fragment; the cc-pV(5,6)Z values are 1.2327 and 1.2325 Å.

Table 2. Bent $C(BH)_2$ isomer: optimized bond lengths (r_e, Å) and angles [°].[a]

	r_e(B−C)	r_e(B−H)	∢(B-C-B)	∢(H-B-C)	r_e(B−B)	∢(C-B-B)
CCSD(T)						
cc-pVDZ	1.3987	1.1911	90.99	175.82	1.9951	44.50
cc-pVTZ	1.3803	1.1749	90.64	176.03	1.9629	44.68
cc-pVQZ	1.3756	1.1739	90.56	176.24	1.9549	44.72
cc-pCVTZ (AE)	1.3761	1.1735	90.57	176.14	1.9556	44.72
cc-pCVQZ (AE)	1.3712	1.1717	90.42	176.35	1.9464	44.79
c~CCSDT(Q)						
cc-pCVQZ(AE)	1.3721	1.1718	90.36	176.32	1.9467	44.82

[a] See footnote [a] of Table 1.

Table 3. Transition state for $C(BH)_2$ isomerization: CCSD(T) optimized bond lengths (r_e, Å) and angles [°].[a]

CCSD(T)/basis	r_e(B−C)	r_e(B−H)	∢(B-C-B)	∢(H-B-C)	r_e(B−B)
cc-pVDZ	1.3853	1.1889	125.84	178.48	2.4668
cc-pVTZ	1.3689	1.1735	124.83	178.49	2.4266
cc-pVQZ	1.3649	1.1725	125.22	178.71	2.4238
cc-pCVTZ (AE)	1.3650	1.1722	124.80	178.62	2.4193
cc-pCVQZ (AE)	1.3608	1.1703	125.17	178.82	2.4160

[a] See footnote [a] of Table 1.

Results and Discussion

Structures, energies, and vibrational spectra: The geometric structures of the closed-shell ground electronic states of the linear and bent isomers of $C(BH)_2$, as well as the transition state (**TS1**) for their interconversion, were optimized at the CCSD(T) level using basis sets ranging from cc-pVDZ to cc-pCVQZ. The resulting geometric parameters are collected in Tables 1, 2, and 3. Figure 1 shows the AE-CCSD(T)/cc-pCVQZ structures in comparison with BP86/TZVPP[37] density functional results.

As expected, the B−C and B−H bond lengths decrease with both basis-set enlargement and inclusion of core correlation, and the QZ basis sets provide results close to the CBS limit. Extrapolation of the bond lengths with a bX^{-3} form as in Equation (2) suggests that in all three $C(BH)_2$ structures the AE-CCSD(T)/cc-pCVQZ values for r_e(B−C) and r_e(B−H) lie about 0.003 and 0.0014 Å above the CBS limit for this level of theory, respectively. The CCSD(T) bond angles in the bent and TS structures do not vary much as the basis set is improved, and convergence to about 0.2° is reached with the QZ basis sets. In Figure 1 it is notable that BP86/TZVPP density functional theory gives substantial errors with respect to AE-CCSD(T)/cc-pCVQZ for the B-C-B angle, namely, +3.0 and −10.8° for the bent and TS forms, respectively.

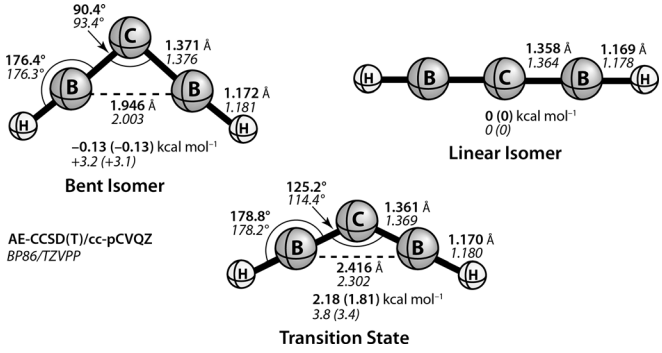

Figure 1. Optimum geometric parameters (Å, °) and relative energies (ΔE_e in kcal mol^{-1}) for the linear (**1a**) and bent (**1b**) isomers of $C(BH)_2$ and the intervening transition state. AE-CCSD(T)/cc-pCVQZ values boldfaced; BP86/TZVPP results in italics; energies (ΔE_0) with zero-point vibrational corrections in parentheses.

From a chemical perspective, the carbon–boron bond length (1.355 Å) in **1a** is very short. This bond length is

much shorter than the standard value for a covalent C=B double bond (1.45 Å),[38] and it is only slightly longer than that for the C≡B triple bond (1.33 Å).[39] Note, however, that the genuine C≡B triple bond in the singlet ($^1\Sigma^+$) HCB molecule has an equilibrium distance of only 1.271 Å at the CCSD(T)/cc-pVTZ level.[40] In comparison, the boron–carbon triple bond length in $HB{\equiv}CH^-$ is predicted to be 1.319 Å at CISD/TZ2P and 1.325 Å at B3LYP/6-311++G**.[41]

Our computations show that **1b** has a remarkably acute B-C-B bending angle close to 90°, the most reliable prediction being 90.4° (AE-CCSD(T)/cc-pCVQZ). The large change in the B-C-B angle from 180° in **1a** to 90° in **1b** is accompanied by a surprisingly small elongation (≈0.013 Å) of the carbon–boron bond length. Even in the isomerization transition state, the B–C length differs by no more than 0.01 Å from the corresponding reactant and product distances. In addition, the B–H bond varies by less than 0.003 Å during the isomerization process, always maintaining a distance about 0.06 Å longer than that in diatomic BH($^1\Sigma^+$) (Table 1). Finally, **1b** exhibits an H-B-C angle that is removed from linearity by less than 4°.

Table 4. Focal-point analysis of the linear→bent isomerization energy [kcal mol^{-1}] of $C(BH)_2$.[a,b]

	ΔE_e(RHF)	$+\delta$ (MP2)	$+\delta$(CCSD)	$+\delta$(CCSD(T))	$+\delta$(CCSDT(Q))	NET
cc-pVDZ	+3.41	−2.71	−1.36	+0.83	+0.32	+0.48
cc-pVTZ	+3.97	−3.52	−1.02	+0.71	+0.33	+0.47
cc-pVQZ	+3.90	−3.70	−1.01	+0.70	[+0.33]	[+0.23]
cc-pV5Z	+3.90	−3.85	−0.99	+0.69	[+0.33]	[+0.07]
cc-pV6Z	+3.89	−3.88	−0.99	+0.69	[+0.33]	[+0.04]
CBS limit	[+3.89]	[−3.91]	[−0.99]	[+0.69]	[+0.33]	[+0.01]
function	$a+be^{-cX}$	$a+bX^{-3}$	$a+bX^{-3}$	$a+bX^{-3}$	addition	
X (fit points) =	(4,5,6)	(5,6)	(5,6)	(5,6)		

[a] FC-CCSD(T)/cc-pVQZ reference geometries: Δ(ZPVE) = −0.011; Δ(core) = +0.020; Δ(DBOC) = +0.005; Δ(rel) = −0.005; ΔE_0(FPA) = +0.01−0.011+0.005−0.005+0.020 = +0.02 kcal mol^{-1}. [b] The symbol δ denotes the increment in the energy difference (ΔE_e) with respect to the previous level of theory in the hierarchy RHF→MP2→CCSD→CCSD(T)→CCSDT(Q). Bracketed numbers result from basis-set extrapolations (using the specified functions and fit points) or additivity approximations, whereas unbracketed numbers were explicitly computed. The main table targets ΔE_e(FC-CCSDT(Q)) in the complete basis-set limit (NET/CBS LIMIT). Auxiliary energy terms are appended for zero-point vibrational energy (ZPVE), core electron correlation (Δ(core)), the diagonal Born–Oppenheimer correction (Δ(DBOC)), and special relativity (Δ(rel)). The final energy difference ΔE_0(FPA) is boldfaced.

The bent isomer does not exhibit a true B–B bond, although some boron–boron covalent interaction can be expected. The B–B interatomic distance of 1.946 Å (AE-CCSD(T)/cc-pCVQZ) in **1b** is much longer than the standard value for a B–B single bond (1.70 Å).[42] Moreover, BP86/TZ2P theory yields a B–B distance in **1b** that is 0.25 Å longer than that in planar $H_2B{-}BH_2$ (1.752 Å).[43] More discussion on this topic appears in the bonding-analysis section below. Our searches did not find an energy minimum for a genuine cyclic form of $C(BH)_2$ exhibiting a B–B single bond.

The relative energies of the linear, bent, and TS structures of $C(BH)_2$ are also given in Table 1 and Figure 1. At the BP86/TZVPP level, **1b** is 3.1 kcal mol^{-1} higher than **1a**, and the barrier for collapsing to **1a** is merely 0.3 kcal mol^{-1}. However, the CCSD(T) results show that BP86/TZVPP significantly underestimates both the thermodynamic and kinetic stability of **1b**. All of the CCSD(T) data in Table 1 place **1b** within 0.2 kcal mol^{-1} of **1a**. In particular, AE-CCSD(T)/cc-pCVQZ theory predicts that the bent isomer is 0.13 kcal mol^{-1} lower in energy.

The linear→bent isomerization energy is pinpointed by the FPA results in Table 4. Therein, full convergence to the CBS limit is achieved, as demonstrated by the nearly exact agreement between the explicitly computed cc-pV6Z increments and the extrapolated values. The convergence toward the electron correlation limit is also excellent; systematic reduction is witnessed in the successive correlation increments, and the final δ(CCSDT(Q)) contribution is only 0.33 kcal mol^{-1}. With inclusion of the auxiliary terms, we find a final FPA isomerization energy of 0.02 kcal mol^{-1} that favors the linear form by a minuscule amount. In fact, this energy difference is less than our estimated uncertainty of ±0.10 kcal mol^{-1}. In essence, the two angle-deformation isomers of $C(BH)_2$ are energetically degenerate.

Figure 2 shows the FPA reaction profile for the rearrangement between **1a** and **1b**. In this diagram, the ZPVE of the low-frequency B-C-B bending mode has been removed from the relative energies to expose the one-dimensional vibrationally adiabatic potential-energy curve on which isomerization occurs. In this representation, **1b** lies 0.01 kcal mol^{-1} above **1a**, and its ground vibrational state ($v=0$) is 0.02 kcal mol^{-1} higher than its linear counterpart. The B-C-B bending angle distorts to 125.2° (AE-CCSD(T)/cc-pCVQZ) in the transition state, which results in a barrier of 2.33 kcal mol^{-1} with respect to the linear form. With inclusion of ZPVE for the reaction mode, the activation barrier is reduced to 1.89 kcal mol^{-1}. The FPA that arrives at this result is laid out in Table 5, in which the basis set and electron correlation series are converged even better than for the isomerization energy in Table 4. Because the barrier separating **1a** and **1b** is so small, these two isomers should rapidly interconvert even at low temperatures.

The thermodynamic stability of $C(BH)_2$ was assessed by computing the total dissociation energy (TDE) for breaking both carbon–boron bonds in **1a** to yield ground-state fragments as shown in Equation (6):

$$\text{linear}\quad C(BH)_2 \rightarrow C(^3P) + 2\,BH(^1\Sigma^+) \qquad (6)$$

Table 6 details the FPA for Equation (6). Because multiple bonds are being homolytically cleaved, the basis set and electron-correlation requirements for computing an accurate TDE are severe. Nonetheless, our FPA is able to arrive at a result, TDE = 294.8 kcal mol^{-1}, that is accurate to better

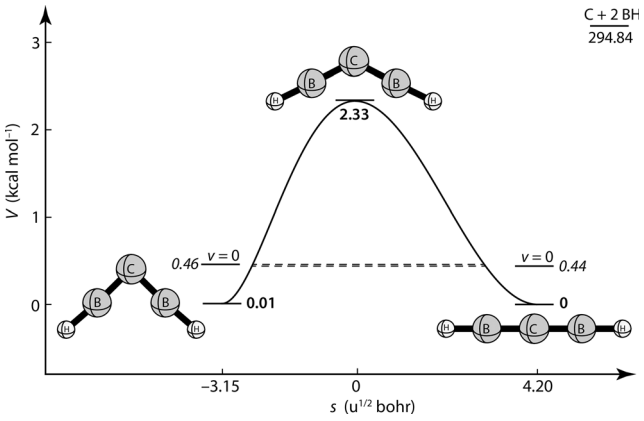

Figure 2. Final FPA energy profile ($V(s)$) versus arc length (s) along the $C(BH)_2$ isomerization path, relative to the energy of the separated fragments $C(^3P)+2\,BH(^1\Sigma^+)$ (not drawn to scale). The boldfaced values correspond to the vibrationally adiabatic potential-energy curve that includes ZPVE for all modes complementary to the reaction coordinate. The ground vibrational levels of the two isomers, containing the ZPVE available to the reaction coordinate, are shown in italics. The abscissa is the arc length in mass-weighted Cartesian coordinate space along the intrinsic reaction path (IRP).

than 1 kcal mol^{-1}. Therefore, we confidently conclude that the mean C–B bond-dissociation energy (D_0) in both $C(BH)_2$ isomers is very large: 147 kcal mol^{-1}. This value is much larger than in the case of HC≡B-($^1\Sigma^+$)→CH($^2\Pi$)+B(^{2}P), for which we computed a precise $D_0(HCB(^1\Sigma^+))=84.9$ kcal mol^{-1} using our FPA method. However, the excitation energies for atomic B(^{2}P→^{2}D) (136.7 kcal mol^{-1})[44] and diatomic CH($^2\Pi\rightarrow{}^4\Sigma^-$) (16.7 kcal mol^{-1}),[45] which are required to obtain the electronic reference state for HC≡B, are much higher than the excitation energy for $2\,BH(^1\Sigma^+\rightarrow{}^3\Pi)$ ($2\times30.3=60.6$ kcal mol^{-1}),[46] which provides the electronic reference state of $C(BH)_2$. The mean intrinsic interaction energy of the carbon–boron bonds in **1a** becomes 178 kcal mol^{-1} when the reference state $C(^3P)+BH(^3\Pi)$ is considered. In comparison, the intrinsic interaction energy for the triple bond in HC≡B with respect to CH($^4\Sigma^-$)+B(^{2}D) is 238.3 kcal mol^{-1}, which is obtained by correcting our aforementioned $D_0(HCB(^1\Sigma^+))$ computed with the FPA method.

The matrix-isolation investigation[9] that produced $C(BH)_2$ and identified it as a linear molecule codeposited methane molecules with pulsed-laser-evaporated boron atoms to create numerous new species. Attention was focused on the 1700–1900 cm^{-1} infrared region because it contained only one new product. Scaled vibrational frequencies computed from a low level of theory (RHF/DZP) aided the assignment of a limited set of experimental IR spectral bands arising from $^{11}B/^{10}B$, H/D, and $^{12}C/^{13}C$ isotopologues. The possibility of a bent $C(BH)_2$ isomer was apparently not considered. The experimental spectra showed three strong IR bands at 1895.2, 1883.9, and 1872.0 cm^{-1} that were assigned to the $\nu_4(\sigma_u^+)$ antisymmetric B=C=B stretching mode of the $H^{10}BC^{10}BH$, $H^{11}BC^{10}BH$, and $H^{11}BC^{11}BH$ species, respectively. Corresponding $\nu_4(\sigma_u^+)$ assignments of 1849.7, 1837.9, and 1825.4 cm^{-1} for $H^{10}B^{13}C^{10}BH$, $H^{11}B^{13}C^{10}BH$, and $H^{11}B^{13}C^{11}BH$ and 1732.2, 1729.8, and 1727.4 cm^{-1} for $D^{10}BC^{10}BD$, $D^{11}BC^{10}BD$, and $D^{11}BC^{11}BD$, respectively, were also made. Finally, a 2230.7, 2213.1, and 2190.9 cm^{-1} set of bands was assigned to the $\nu_3(\sigma_u^+)$ antisymmetric B–D stretching mode of $D^{10}BC^{10}BD$, $D^{11}BC^{10}BD$, and $D^{11}BC^{11}BD$, respectively. No additional bands of linear $C(BH)_2$ were assigned to other regions of the IR spectrum.

The CCSD(T) and c~CCSDT(Q) harmonic (ω_i) and anharmonic (ν_i) vibrational frequencies of the parent $^{12}C/^{11}B/H$ isotopologue computed in this study for the linear, bent, and transition-state structures of $C(BH)_2$ are collected in Table 7, in which good convergence is seen with respect to the level of theory. In Tables S3–S12 of the Supporting

Table 6. Focal-point analysis of the reaction energy [kcal mol^{-1}] for linear $C(BH)_2\rightarrow C(^3P)+2\,BH(^1\Sigma^+)$.[a,b]

	ΔE_e(RHF)	$+\delta$(CCSD)	$+\delta$(CCSD(T))	$+\delta$ (CCSDT(Q))	NET
cc-pVDZ	+235.96	+31.70	+8.59	+0.72	+276.97
cc-pVTZ	+240.84	+41.87	+10.27	+0.54	+293.52
cc-pVQZ	+241.50	+46.05	+10.71	[+0.54]	[+298.79]
cc-pV5Z	+241.59	+47.35	+10.85	[+0.54]	[+300.32]
cc-pV6Z	+241.56	+47.91	+10.90	[+0.54]	[+300.91]
CBS limit	[+241.55]	[+48.67]	[+10.97]	[+0.54]	[+301.73]
function	$a+be^{-cX}$	$a+bX^{-3}$	$a+bX^{-3}$	addition	
X (fit points)=	(4,5,6)	(5,6)	(5,6)		

[a] FC-CCSD(T)/cc-pVQZ reference geometries: Δ(ZPVE)=−10.413; Δ(core)=+3.019; Δ(DBOC)=+0.276; Δ(rel)=−0.214; ΔE_0(FPA)=+301.73−10.413−0.765−0.214+3.019=+294.84 kcal mol^{-1}. [b] See footnote of Table 4 for notation.

Table 5. Focal-point analysis of the barrier height [kcal mol^{-1}] for linear→bent isomerization of $C(BH)_2$.[a,b]

	ΔE_e(RHF)	$+\delta$ (MP2)	$+\delta$(CCSD)	$+\delta$(CCSD(T))	$+\delta$(CCSDT(Q))	NET
cc-pVDZ	+1.91	+0.91	−0.99	+0.61	+0.18	+2.61
cc-pVTZ	+2.18	+0.46	−0.85	+0.56	+0.20	+2.56
cc-pVQZ	+2.10	+0.36	−0.88	+0.57	[+0.20]	[+2.35]
cc-pV5Z	+2.10	+0.26	−0.88	+0.57	[+0.20]	[+2.26]
cc-pV6Z	+2.10	+0.24	−0.88	+0.57	[+0.20]	[+2.24]
CBS limit	[+2.10]	[+0.22]	[−0.88]	[+0.57]	[+0.20]	[+2.21]
function	$a+be^{-cX}$	$a+bX^{-3}$	$a+bX^{-3}$	$a+bX^{-3}$	addition	
X (fit points)=	(4,5,6)	(5,6)	(5,6)	(5,6)		

[a] FC-CCSD(T)/cc-pVQZ reference geometries: Δ(ZPVE)=−0.378; Δ(core)=+0.054; Δ(DBOC)=+0.002; Δ(rel)=−0.003; ΔE_0(FPA)=+2.21−0.378+0.002−0.003+0.054=+1.89 kcal mol^{-1}. [b] See footnote of Table 4 for notation.

Table 7. Harmonic (ω_i) and anharmonic (ν_i) vibrational frequencies [cm^{-1}] and IR intensities ($km\,mol^{-1}$, in parentheses) of stationary points of $C(BH)_2$ computed with several basis sets.[a]

Mode (sym)	Description[b]	c-pVTZ CCSD(T) ω_i	cc-pVQZ CCSD(T) ω_i	cc-pCVQZ CCSD(T) ω_i	cc-pCVQZ c~CCSDT(Q) ω_i	cc-pVTZ CCSD(T) ν_i	cc-pCVQZ c~CCSDT(Q) ν_i
Linear $C(BH)_2$							
1 (σ_g^+)	sym B–H stretch	2834 (0)	2839 (0)	2846 (0)	2844	2734	2743
2 (σ_g^+)	sym B–C stretch	1118 (0)	1121 (0)	1126 (0)	1122	1113	1119
3 (σ_u^+)	asym B–H stretch	2843 (141)	2851 (141)	2858 (140)	2857	2744	2752
4 (σ_u^+)	asym B–C stretch	1902 (427)	1905 (437)	1913 (440)	1905	1874	1875
5 (π_g)	asym H-B-C bend	751 (0)	754 (0)	756 (0)	752	746	751
6 (π_u)	sym H-B-C bend	727 (28)	734 (29)	738 (29)	733	723	732
7 (π_u)	B-C-B bend	166 (36)	154 (37)	154 (37)	158	151	153
Bent $C(BH)_2$							
1 (a_1)	sym B–H stretch	2811 (13)	2816 (12)	2824 (12)	2822	2708	2714
2 (a_1)	sym B–C stretch	1414 (11)	1423 (12)	1432 (12)	1428	1386	1395
3 (a_1)	sym H-B-C ip bend	769 (3)	772 (3)	775 (3)	772	766	768
4 (a_1)	B-C-B bend	315 (0.02)	317 (0.02)	320 (0.03)	318	287	289
5 (a_2)	asym H-B-C oop bend	774 (0)	783 (0)	786 (0)	784	769	775
6 (b_1)	sym H-B-C oop bend	719 (3)	729 (3)	732 (3)	729	716	722
7 (b_2)	asym B–H stretch	2809 (57)	2815 (54)	2823 (52)	2821	2704	2715
8 (b_2)	asym B–C stretch	1536 (84)	1543 (85)	1551 (85)	1545	1525	1537
9 (b_2)	asym H-B-C ip bend	791 (12)	796 (12)	799 (11)	797	785	788
$C(BH)_2$ transition state							
1 (a_1)	sym B–H stretch	2824	2831	2838			
2 (a_1)	sym B–C stretch	1275	1280	1288			
3 (a_1)	sym H-B-C ip bend	743	751	754			
4 (a_1)	B-C-B bend	176*i*	173*i*	175*i*			
5 (a_2)	asym H-B-C oop bend	748	757	759			
6 (b_1)	sym H-B-C oop bend	721	732	736			
7 (b_2)	asym B–H stretch	2832	2839	2846			
8 (b_2)	asym B–C stretch	1770	1777	1785			
9 (b_2)	asym H-B-C ip bend	762	770	772			

[a] (FC, AE) CCSD(T) for the cc-pV*X*Z and cc-pCV*X*Z basis sets; IR intensities are double-harmonic values. [b] Abbreviations: sym = symmetric; asym = antisymmetric; ip = in-plane; oop = out-of-plane.

Information, harmonic and anharmonic frequencies for the CCSD(T)/cc-pVTZ, CCSD(T)/cc-pCVQZ, and c~CCSDT(Q)/cc-pCVQZ levels of theory are tabulated for a full set of 12 isotopologues arising from ^{13}C, ^{10}B, and D substitutions. Figure 3 illustrates the c~CCSDT(Q)/cc-pCVQZ infrared spectrum corresponding to natural isotopic abundances and an equimolar mixture of the linear and bent isomers.

The linear and bent isomers exhibit characteristic differences in their vibrational spectra that could make it possible to identify both species through IR spectroscopy. The anharmonic c~CCSDT(Q)/cc-pCVQZ spectrum for linear $H^{11}B^{12}C^{11}BH$ shows strong signals at 1875 and 2752 cm^{-1} for the antisymmetric B=C=B and B–H stretches, respectively; the corresponding absorption frequencies for $D^{11}B^{12}C^{11}BD$ are 1730 and 2193 cm^{-1}. These results are in very close agreement with the recorded IR spectrum of Hassanzadeh and Andrews,[9] deviating by only 2–3 cm^{-1}. In Table 8, CCSD(T)/cc-pVTZ and c~CCSDT(Q)/cc-pCVQZ isotopic shifts of the ν_3 and ν_4 fundamental frequencies of linear $C(BH)_2$ are listed alongside the observed values.[9] The

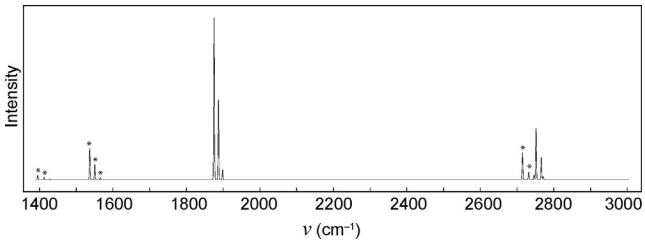

Figure 3. Simulated IR spectrum in the 1400–3000 cm^{-1} region of an equimolar mixture of linear and bent $C(BH)_2$ in natural isotopic abundances, based on c~CCSDT(Q)/cc-pCVQZ anharmonic frequencies and AE-CCSD(T)/cc-pCVQZ harmonic intensities. Asterisks denote absorptions of the bent isomer.

agreement between theory and experiment is spectacular, further confirming the matrix-isolation assignments.

The theoretical IR spectrum of **1b** contains only two fundamental frequencies with substantial intensity, ν_7(asym B–H str) = 2715 cm^{-1} and ν_8(asym B–C str) = 1537 cm^{-1} (c~CCSDT(Q)/cc-pCVQZ, Table 7). The ν_8 frequency is considerably downshifted by 338 cm^{-1} compared to the antisymmetric B–C stretch of the linear isomer, whereas the corre-

Table 8. Isotopic shifts ($\Delta\nu$, cm^{-1}) of anharmonic vibrational frequencies of linear HBCBH.

		$\Delta\nu$ (CCSD(T)/cc-pVTZ, c~CCSDT(Q)/cc-pCVQZ, matrix isolation[9])		
		$^{11}B/^{11}B$	$^{11}B/^{10}B$	$^{10}B/^{10}B$
$\nu_3(\sigma_u^+)$	DB=C=BD	0, 0, 0	22.4, 22.4, 22.2	39.7, 39.5, 39.8
$\nu_4(\sigma_u^+)$	HB=C=BH	0, 0, 0	11.9, 11.9, 11.9	23.2, 23.2, 23.2
	HB=^{13}C=BH	−46.6, −46.7, −46.6	−34.1, −34.1, −34.1	−22.3, −22.3, −22.3
	DB=C=BD	−146.9, −145.4, −144.6	−144.5, −143.0, −142.2	−142.2, −140.7, −139.8

sponding downshift for ν_7 is 37 cm^{-1}. Although certainly observable, the ν_7 and ν_8 absorptions of **1b** are predicted to have only 37 and 19% of the intensity of their **1a** counterparts, respectively. Thus, a critical question regarding the spectroscopic identification of **1b** is whether this isomer can be produced in sufficient quantities. This question must now be addressed.

Quantum tunneling of the heavy-atom framework of $C(BH)_2$ is responsible for rapid interconversion between the linear and bent isomers, even at cryogenic temperatures. To establish this isomerization mechanism, the FC-CCSD(T)/cc-pVTZ method was employed to precisely map out the associated intrinsic reaction path (IRP) and to determine zero-point vibrational energies (ZPVEs) along this steepest-descent route. The potential-energy curve $V(s)$ along the IRP was constructed as a function of arc length (s) in mass-weighted Cartesian coordinates by computing AE-CCSD(T)/cc-pCVQZ energy points appended with the aforementioned ZPVEs. Finally, a hyperbolic tangent switching function was used to slightly adjust the barrier height and reaction energy by 0.046 and 0.148 kcal mol^{-1}, respectively, to match the key features of $V(s)$ with the FPA energetics. Figure 2 shows a quantitative plot of the final $V(s)$ function.

Exact probabilities (κ_{exact}) for tunneling through the $V(s)$ barrier profile were evaluated by numerically integrating time-independent, complex-valued wave functions through the barrier and applying the proper boundary conditions for incoming, reflected, and transmitted waves. In addition, WKB (Wentzel–Kramers–Brillouin) tunneling probabilities (κ_{WKB}) were obtained by numerically evaluating barrier penetration integrals (θ) over the final $V(s)$ function.[47] This first-principles approach to quantifying tunneling rates has proved very effective in recent studies of hydroxycarbenes.[48–50]

The reactant normal mode leading from bent to linear $C(BH)_2$ has the harmonic vibrational frequency ω_4(B-C-B bend) = 320 cm^{-1} (AE-CCSD(T)/cc-pCVQZ, Table 7). Therefore, collisions of **1b** with the isomerization barrier occur with a 0 K energy $\varepsilon = \omega_4/2 = 160$ cm^{-1} in the reaction coordinate. The tunneling rate for isomerization can be computed as the product of the transmission coefficient ($\kappa(\varepsilon)$) and the classical rate (ω_4) at which the reactant hits the barrier. Employing κ_{exact} and κ_{WKB} reveals a half-life ($t_{1/2}$) of only 0.010 and 0.012 s for tunneling from the ground vibrational state of the bent isomer to the linear form. Performing the same analysis for reverse tunneling of **1a** back to **1b** yields $t_{1/2} = 0.016$ and 0.021 s based on κ_{exact} and κ_{WKB}, respectively. If the AE-CCSD(T)/cc-pCVQZ curve for the IRP is used without final adjustment to match the FPA energetics, the same linear↔bent interconversion half-lives range only from 0.005 to 0.050 s. The picture that emerges, regardless of the details of the theoretical analysis, is that the two isomers of $C(BH)_2$ can interconvert by heavy-atom tunneling on a timescale much less than 1 s even in the complete absence of thermal energy.

To discern the longest possible period over which a viable isotopologue of the bent form could persist in isolation prior to isomerization, we applied our tunneling analysis to ^{13}C-($^{11}BD)_2$. The IRP was explicitly mapped out again with the heavier masses, and the $V(s)$ curve was reconstructued with new energy points. The WKB tunneling result was $t_{1/2} = 3.8$ s, which highlights the inherent evanescent nature of the bent species.

Rapid tunneling between the linear and bent isomers may allow an equilibrium to be reached between these species in cryogenic matrices. At the temperature (12 K) of the matrix-isolation experiments of refs. [9] and [51], the Boltzmann factor (f_B) representing the bent/linear population ratio is 0.55 based on the FPA energy difference ($\Delta E_0 = +0.014$ kcal mol^{-1}). The ratio of the greatest IR intensities in the vibrational spectra of these isomers is $f_{IR} = 0.19$ ($I(\omega_8$ bent)/$I(\omega_4$ linear), AE-CCSD(T)/cc-pCVQZ, Table 7). Therefore, in an equilibrium mixture at 12 K, the signal of the strongest IR band of the bent isomer would be only a fraction $f = f_B f_{IR} = 0.11$ of the signal coming from the linear species. If matrix effects and residual errors in the FPA energy predictions were to shift ΔE_0 by +0.05 and −0.05 kcal mol^{-1}, very reasonable scenarios, f would be reduced/increased to 0.01 and 0.86, respectively. These rough estimates assist in the interpretation of the matrix-isolation experiments. The comprehensive 1993 paper[51] that followed the preliminary report of Hassanzadeh and Andrews[9] showed the entire 500–1900 cm^{-1} region of the infrared spectrum obtained after codepositing laser-ablated boron atoms with Ar/CH_4. A broad, weak feature in the vicinity of 1550 cm^{-1} is unassigned. Because the intensity of this band does not correlate well with changes in the **1a** signals upon either UV radiation or annealing of the matrix, the absorption probably does not arise primarily from **1b** and serves to mask any signal from this isomer. In summary, our computations show that it is quite possible that a significant fraction of $C(BH)_2$ exists in the Ar matrix as the bent isomer, but the associated IR signals are inherently more difficult to detect and are obscured by other species.

Bonding analysis: The bonding in **1a** and **1b** was analyzed with various methods to explain the unusual occurrence of two nearly isoenergetic angle-deformation isomers. The investigation tested the hypothesis that the linear form exhibits C−B electron-sharing bonds, whereas the bent isomer is

characterized by HB→C←BH coordinate covalent, donor–acceptor interactions in which the carbon atom retains two lone pairs. An atoms-in-molecules (AIM)[52] analysis of the electronic structure was carried out first. Figure 4 shows the

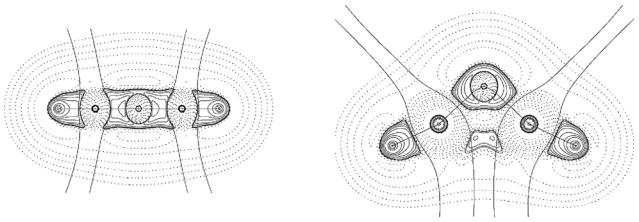

Figure 4. Contour line diagrams $\nabla^2\rho(\mathbf{r})$ of a) linear $C(BH)_2$ and b) bent $C(BH)_2$. Solid lines indicate areas of charge concentration ($\nabla^2\rho(\mathbf{r})<0$) and dashed lines show areas of charge depletion ($\nabla^2\rho(\mathbf{r})>0$). The thick solid lines connecting the atomic nuclei are the bond paths. The thick solid lines separating the atomic basins indicate the zero-flux surfaces crossing the molecular plane. Electron density $\rho(\mathbf{r}_c)$, Laplacian $\nabla^2\rho(\mathbf{r}_c)$, and total energy density $H(\mathbf{r}_c)$ at the C–B bond critical points.

contours of the Laplacian $\nabla^2\rho(\mathbf{r})$ of the electron density of the two isomers in the molecular plane.

In both **1a** and **1b**, C–B and B–H bond paths exist as expected, but no B–B bond path is observed in the bent isomer. The Laplacian of both isomers exhibits large areas of internuclear charge concentration ($\nabla^2\rho<0$, solid lines) indicative of C–B electron-sharing bonds. The area of charge concentration below the carbon atom and between the boron atoms in **1b** suggests some covalent B–B interaction, but not strong enough to yield a bond path.[53] The possible strength of the B–B interaction was gauged by computing the energy difference between the $(BH)_2$ system at the frozen geometry of **1b** and two separated BH diatomics. This measure yields significant boron–boron attraction in bent $C(BH)_2$, 54.1 and 48.9 kcal mol^{-1} at BP86/TZVPP and CCSD(T)/TZVPP//BP86/TZVPP, respectively. However, the discussion below shows that it is difficult to separate direct boron–boron bonding from three-center CB_2 bonding in **1b**.

The position of the C–B bond critical point (bcp) evidences strong polarization towards carbon in both isomers (Figure 4). Likewise, NBO analysis gives a large negative charge on carbon in the linear form ($-1.49\,e$) and the bent isomer ($-0.98\,e$). The charge density, Laplacian $\nabla^2\rho$, and energy H at the bcp of the C–B bonds are all similar in the two isomers. Moreover, the shape of the Laplacian distribution at the carbon atom in bent $C(BH)_2$ is not typical for lone-pair electrons. Collectively, these results show that the C–B bonding is not very different in **1a** and **1b**, and the donor–acceptor interpretation of the bonding in bent $C(BH)_2$ is not supported.

Figure 5 depicts the valence orbitals of the two isomers. The degenerate π HOMO of **1a** is split into the energetically similar π HOMO(b_1) and σ HOMO−1(a_1) of **1b**. The π HOMO of **1b** has the same shape as the lowest-lying π molecular orbital of the allyl system. The σ HOMO−1 has the largest contribution from the p(σ) atomic orbital (AO) of carbon, the backside lobe of which overlaps in-phase with the in-plane sp-hybridized AOs of boron. Thus, the HOMO−1 further strengthens the B–C bonds and also contributes some B–B bonding. A similar shape was found for the HOMO−1 of the substituted homologues $C(ECp^*)_2$ (Al to Tl), attesting to some E–E attraction.[7] The electron-density profile of the HOMO−1 accounts for the rather acute central bond angles in $C(ECp^*)_2$ (Al to Tl) and **1b**. This density is visible in the area of charge concentration between the boron atoms in the Laplacian distribution of bent $C(BH)_2$ (Figure 4b). The lower-lying valence orbitals of **1b** directly correlate with the associated valence orbitals of **1a**.

The bonding in linear and bent $C(BH)_2$ may thus become interpreted as follows. The linear isomer is a cumulene HB=C=BH with classical electron-sharing σ/π double bonds (Figure 6a) in which the π bonding comes from two three-center

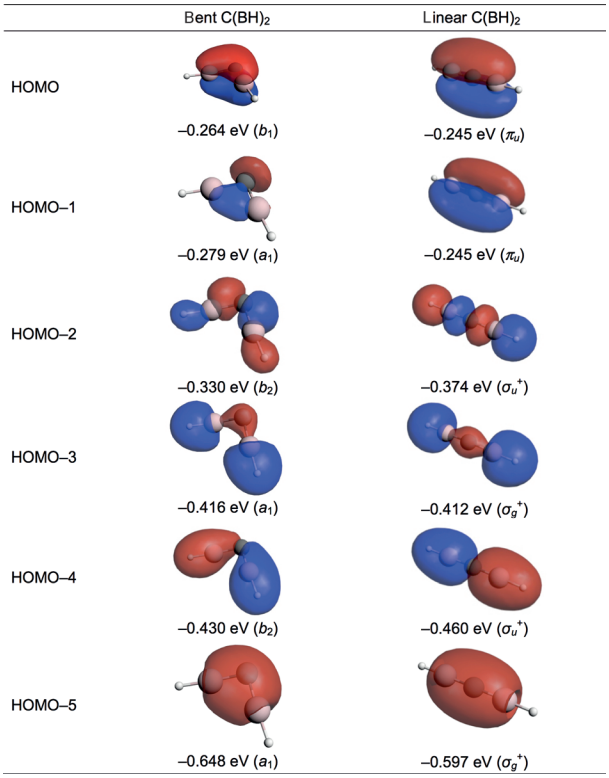

Figure 5. Shape and eigenvalues of the valence orbitals of linear and bent $C(BH)_2$.

two-electron bonds. Thus, each C–B π bond extends over the entire B-C-B framework, which explains why the C–B bond length in the linear form is shorter than that of a standard double bond. However, from the traditional bonding perspective the boron atoms in **1a** have only six electrons in their valence shells. This viewpoint suggests that partially gaining an electron octet around the boron atoms might be a driving force for forming the bent isomer. The process is shown schematically in Figure 6b, which depicts an initial carbone HB→C←BH reference structure, whose carbon σ lone pair is subsequently donated into the empty in-plane p AOs of boron. An alternative view is provided by a cyclic $C(BH)_2$ reference structure with an "inverted" carbene[54] configuration that donates charge into the vacant carbon σ lone-pair orbital (Figure 6c).[55] Both perspectives come to

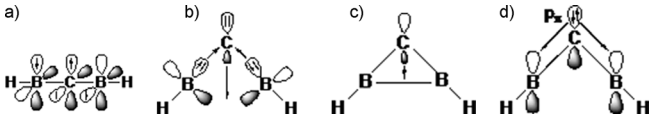

Figure 6. Qualitative models for explaining the shape of the HOMO and HOMO-1 of bent $C(BH)_2$. a) Cumulene bonding with electron-sharing σ/π bonding in linear HB=C=BH (**1a**). The sketches b) and c) give two different perspectives for the explanation of the HOMO−1 of **1b**. Depiction b) starts from a carbone reference point while c) starts from $C(BH)_2$ as reference structure where the p(π) AO of carbon is doubly occupied and the σ AO is vacant ("inverted carbene"). d) π-Backdonation of the occupied p(π) AO of carbon into the vacant p(π) AOs of the boron atoms.

the same conclusion: the HOMO−1 in bent $C(BH)_2$ enhances carbon–boron bonding, it yields partial boron–boron bonding, and it has some (reduced) σ lone-pair character. Finally, Figure 6d shows the π back-donation from the occupied p(π) AO of carbon into the empty p(π) AOs of boron. The shape of the HOMO (Figure 5) suggests that the C→BH π back-donation is very strong, which considerably weakens the lone-pair character at carbon.

The lack of strong carbone character in bent $C(BH)_2$ is revealed by computing first and the second proton affinities (PAs). It has been shown before that carbones have exceptionally high second PAs, because they have two lone pairs available for protonation in contrast to carbenes.[1] Typical carbones CL_2 with $L=PR_3$ (carbodiphosphoranes) and $L=$ N-heterocyclic carbene (NHC) (carbodicarbenes) have a first PA of 280–300 kcal mol^{-1} whereas the second PA is 150–190 kcal mol^{-1}.[56] With CCSD(T)/TZVPP, the first PA of bent $C(BH)_2$ is 190.9 kcal mol^{-1} whereas the second PA is only 35.4 mol^{-1}. These results are more characteristic for a carbene than a carbone.

URVA analysis

Analysis of isomers using local vibration modes and force constants: Information on the electronic structure of a molecule and its bonding is encoded in the normal vibrational modes. However, normal modes tend to be delocalized as a result of coupling of local modes. Therefore, only the latter can provide detailed insight into the different bonding and electronic structure of isomers such as **1a** and **1b**. Recent work[57,58] has proved that the local vibrational modes of Konkoli and Cremer[59] represent a unique set of local modes directly related to the normal vibrational modes by means of an adiabatic connection scheme (ACS). The change of a local-mode frequency ω_a from the corresponding normal-mode frequency ω_μ in an ACS is measured by the coupling frequency [Eq. (7)], which absorbs all mass-coupling effects with all other $N_{vib}-1$ local modes. The sum of all $|\omega_{coup}|$ adopts a minimum if the set of local vibrational modes is unique.[57]

$$\omega_{coup} = \omega_a - \omega_\mu \qquad (7)$$

In Figures 7 and 8 the adiabatic connection scheme for **1a** and **1b**, respectively, is shown as the fractional coupling parameter (λ) varies from 0 to 1. For **1a**, four bond lengths ($(B-H)_{1,2}$, $(B-C)_{1,2}$) and three pairs of linear bending angles ($(H\text{-}B\text{-}C)_{1a,1b}$, $(H\text{-}B\text{-}C)_{2a,2b}$, $(B\text{-}C\text{-}B)_{ab}$) give the best match between normal and local vibrational modes. For **1b**, four bond lengths ($(B-H)_{1,2}$, $(B\text{-}C)_{1,2}$), three bond angles ($(H\text{-}B\text{-}C)_{1,2}$, $(B\text{-}C\text{-}B)$), and two torsional angles ($(H\text{-}B\text{-}C\text{-}B)_{1,2}$) lead to the lowest coupling frequencies. In Table 9, AE-CCSD(T)/cc-pCVQZ local-mode, normal-mode, and coupling frequencies (ω_a, ω_μ, ω_{coup}) are given for **1a** and **1b** along with the local-mode decomposition of the normal modes according to Konkoli and Cremer.[60] The ACSs reveal that for both **1a** and **1b** the mass coupling is small for all bending motions and the B−H stretching motions. There is, however, a significant difference between the isomers for the B−C stretching modes. In general, a central bond angle of 90° suppresses couplings between neighboring stretches, whereas a bond angle of 0 or 180° leads to the strongest coupling.[57] Because the B-C-B angle in **1b** is very close to 90°, the local B−C stretches are only weakly coupled. The local $\omega_a(B-C)_{1,2}$ stretching frequencies of 1522 cm^{-1} transform into the symmetric and antisymmetric B−C normal-mode frequencies ($\omega_2(a_1)=1432$ cm^{-1}, $\omega_8(b_2)=$

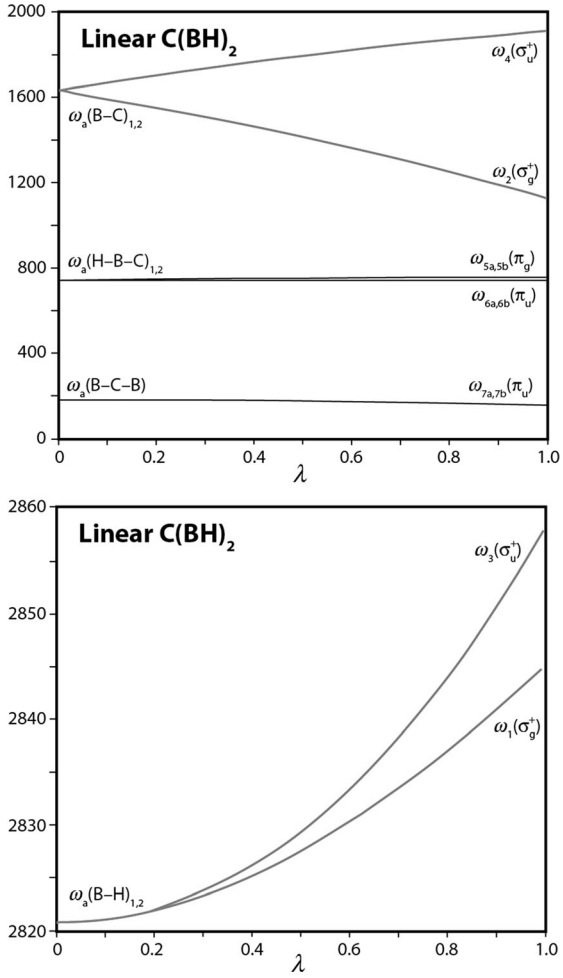

Figure 7. Adiabatic connection scheme for **1a** showing the transformation of local (ω_a) to normal (ω_μ) mode vibrational frequencies (AE-CCSD(T)/cc-pCVQZ, in cm^{-1}) as the scale factor λ varies from 0 to 1.

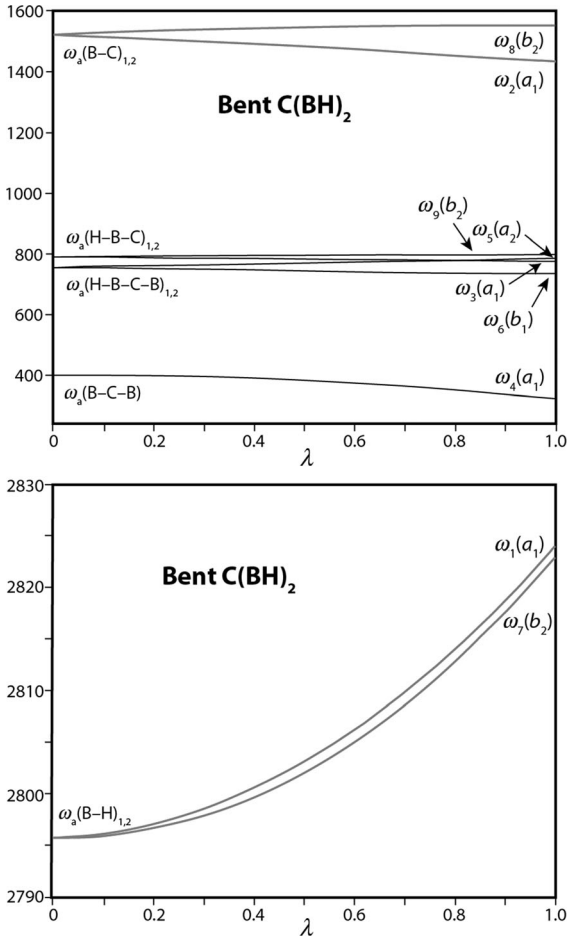

Figure 8. Adiabatic connection scheme for **1b** showing the transformation of local (ω_a) to normal (ω_μ) mode vibrational frequencies (AE-CCSD(T)/cc-pCVQZ, in cm^{-1}) as the scale factor λ varies from 0 to 1.

1551 cm^{-1}) as a result of $\omega_{coup} = -90$ and 29 cm^{-1}. In contrast, for **1a** the B-C-B angle of 180° should lead to strong coupling, as fully confirmed by the ACS. Considerably larger **1a** coupling frequencies of −504 and 283 cm^{-1} transform the local ω_a-$(B{-}C)_{1,2}$ stretching frequencies of 1630 cm^{-1} into the symmetric and antisymmetric B–C normal-mode frequencies (ω_2-$(\sigma_g^+) = 1126$ cm^{-1}, $\omega_4(\sigma_u^+) = 1913$ cm^{-1}).

Measures of the B–C and B–H bond strengths in **1a** and **1b** must be obtained from local-mode rather than normal-mode properties. Local-mode adiabatic stretching force constants (k_a) provide a direct measure of bond strengths[60] devoid of the mass effects. These force constants can be converted into more interpretable bond-order parameters (n) with the help of suitable reference molecules (Scheme 1).[61–64] For this purpose we assume the reference bond orders $n_{BC} = 1$ for CH_3BH_2 (**2**), $n_{BC} = 2$ for $H_2C{=}BH$ (**3**), $n_{BB} = 1$ for $C_4B_2H_{10}$ (**4**) (diborocyclohexane), $n_{BB} = 2$ for HB=BH (**5**), $n_{BH} = 1$ for BH_3 (**6**), and $n_{BH} = {}^1/_2$ for B_2H_6 (**7**) (electron deficient bonding in H-B-H bridges). Accordingly, the following power relationships are obtained from the B3LYP/6-31G(d,p) data in Table 10 [Eqs. (8)–(10)]:

$$n_{BC} = 0.297\ k_a(B{-}C)^{0.907} \quad (8)$$

$$n_{BB} = 0.363\ k_a(B{-}B)^{0.984} \quad (9)$$

$$n_{BH} = 0.286\ k_a(B{-}H)^{0.921} \quad (10)$$

As discussed in the section above, the π bonding in **1a** results for two two-electron three-center B–C bonds, which together with the σ bonding should lead to a bond order significantly larger than 2. In **1b** the loss of π bonding is balanced to a large extent by C→B π back-donation, but the B–C bond order should be somewhat smaller than in **1a**. These expectations are confirmed in Table 10, in which $n_{BC} = 2.25$ for **1a** and $n_{BC} = 2.03$ for **1b**. The bond order $n_{BC} = 2.18$ for **TS1** is closer to **1a** than **1b**, which is consistent with the bond lengths in Figure 1. The B–C bond orders for molecules **8**–**12** (Scheme 1, Table 10) further demonstrate the usefulness of the relation in Equation (8).

The B–H bond orders n_{BH} for **1a** (1.12), **1b** (1.10), and **TS1** (1.11) are quite similar, and greater than those in BH_3. It is particularly interesting to derive a bond order for the B–B interaction. As reflected by the values $n_{BB} = 0.085$ for **TS1** and 0.123 for **1b** in Table 10, the bent form has a stabi-

Table 9. Vibrational analysis of **1a** and **1b** applied to CCSD(T)/cc-pCVQZ harmonic vibrational normal-mode frequencies ω_μ.

Type	ω_a [cm^{-1}]	μ	ω_μ [cm^{-1}]	ω_{coup} [cm^{-1}]	Local mode contributions to normal mode [%]
Isomer **1a**					
$\omega_a(B{-}H)_1$	2821	3	2858	37	48 $(B{-}H)_1$ + 48 $(B{-}H)_2$
$\omega_a(B{-}H)_2$	2821	1	2846	24	49 $(B{-}H)_1$ + 49 $(B{-}H)_2$
$\omega_a(B{-}C)_1$	1630	4	1913	282	48 $(B{-}C)_1$ + 48 $(B{-}C)_2$
$\omega_a(B{-}C)_2$	1630	2	1126	−504	49 $(B{-}C)_1$ + 49 $(B{-}C)_2$
ω_a(H-B-C)$_1$	746	5a, 5b	756	10	50 (H-B-C)$_1$ + 50 (H-B-C)$_2$
ω_a(H-B-C)$_2$	746	6a, 6b	738	−8	49 (H-B-C)$_1$ + 49 (H-B-C)$_2$
ω_a(B-C-B)	178	7a, 7b	154	−24	100 (B-C-B)
ZPVE[a]	17.50		17.21	−0.29	
Isomer **1b**					
$\omega_a(B{-}H)_1$	2796	1	2824	28	49 $(B{-}H)_1$ + 49 $(B{-}H)_2$
$\omega_a(B{-}H)_2$	2796	7	2823	27	49 $(B{-}H)_1$ + 49 $(B{-}H)_2$
$\omega_a(B{-}C)_1$	1522	8	1551	29	48 $(B{-}C)_1$ + 48 $(B{-}C)_2$
$\omega_a(B{-}C)_2$	1522	2	1432	−90	48 $(B{-}C)_1$ + 48 $(B{-}C)_2$
ω_a(H-B-C)$_1$	791	9	799	8	50 (H-B-C)$_1$ + 50 (H-B-C)$_2$
ω_a(H-B-C-B)$_1$	757	5	786	29	50 (HBCB)$_1$ + 50 (HBCB)$_2$
ω_a(H-B-C)$_2$	791	3	775	−16	47 (H-B-C)$_1$ + 47 (H-B-C)$_2$ + 5 (B-C-B)
ω_a(H-B-C-B)$_2$	757	6	732	−25	50 (HBCB)$_1$ + 50 (HBCB)$_2$
ω_a(B-C-B)	401	4	320	−81	97 (B-C-B)
ZPVE[a]	17.34		17.21	−0.13	

[a] The ZPVE [kcal mol^{-1}] is added to verify that the sum of local-mode frequencies plus the sum of coupling frequencies equals the sum of normal-mode frequencies.

Table 10. Comparative B3LYP/6-31G(d,p) bond lengths r [Å], associated frequencies ω_μ [cm^{-1}], and adiabatic stretching force constants k_a (mdyn Å^{-1}), and bond orders n of species **1**–**12**.[a]

Species	B–C bond				B–B bond				B–H bond			
	r	ω_μ	k_a	n	r	ω_μ	k_a	n	r	ω_μ	k_a	n
1a	1.358	–	9.352	2.25	–	–	–	–	1.171	–	4.399	1.12
TS1	1.363	1631	8.999	2.18	2.335	266	0.229	0.085	1.173	2830	4.358	1.11
1b	1.370	1567	8.307	2.03	2.031	321	0.334	0.123	1.174	2817	4.318	1.10
2	1.558	1063	3.820	1	–	–	–	–	1.197	2626	3.752	–
3	1.381	1557	8.205	2	–	–	–	–	1.174	2825	4.343	–
4	1.527	1058	3.789	–	1.517	1010	3.305	1	–	–	–	–
5	–	–	–	–	1.525	1322	5.667	2	1.174	–	4.319	–
6	–	–	–	–	–	–	–	–	1.192	2673	3.886	1
7	–	–	–	–	1.769	844	2.312	–	1.316	1834	1.831	0.5
8	1.405	1349	6.160	–	1.588	999	3.235	–	–	–	–	–
9	1.416	1429	6.905	–	2.499	386	0.483	–	1.171	2859	4.445	–
10	–	–	–	–	1.495	1232	4.923	–	1.182	2747	4.104	–
					1.604[b]	985	3.147	–	–	–	–	–
11[c]	1.359	1665	9.379		–	–	–	–	–	–	–	–
12[c]	–	–	–	–	1.618	1014	3.278	–	–	–	–	–

[a] Bond orders n calculated according to Equations (8), (9), and (10) using references **2**, **3** for B–C bonds, **6**, **7** for B–B bonds, and **4**, **5** for B–H bonds. [b] BH–B bonds. [c] Triplet ground state.

lizing B–B interaction, which will be further quantified in the next section.

URVA analysis of the isomerization mechanism: The unified reaction valley analysis (URVA)[65,66] was applied to elucidate the **1a**→**1b** isomerization. Curvature $\mathbf{k}(s)$ and direction $\mathbf{t}(s)$ vectors of the isomerization path as a function of the arc length s were computed using both MP2 and B3LYP theory with the 6-31G(d,p) basis set. According to the reaction-phase concept of Kraka and Cremer,[62] chemical processes such as bond cleavage/formation are indicated by curvature maxima along the reaction path. The generation of a new (transient) electronic structure is finished when the reaction-path curvature adopts a minimum (low chemical activity) after having passed through a curvature maximum (high chemical activity). Hence, a reaction phase is defined as the reaction path range from one curvature minimum (start of the chemical process) to the next (end of a chemical process), which is characterized by an intervening curvature peak. Different chemical reactions possess different curvature patterns and numbers of reaction phases, which can be used as fingerprints.

Further insight into the transformation from **1a** to **1b** can be gained by decomposition of the scalar reaction-path curvature and direction into contributions $A_{n,s}(\mathbf{k};s)$ and $A_{n,s}(\mathbf{t};s)$, respectively, from each local mode n. Figure 9 shows the $\mathbf{k}(s)$ decomposition for the **1a**→**1b** reaction path, whereas Figure S1 in the Supporting Information provides the corresponding $\mathbf{t}(s)$ plot. The local-mode coupling coefficients identify the internal coordinates that dominate the chemical reaction at a given point and reveal the associated chemical changes, such as bond cleavage/formation or rehybridization. Furthermore, the sign of $A_{n,s}(\mathbf{k};s)$ determines whether changes in the structural parameter in question are promoting (positive sign) or hindering (negative sign) the reaction. Because curvature $\mathbf{k}(s)$ and direction $\mathbf{t}(s)$ are orthogonal to each other, their decomposition into local vibrational modes is complementary. Generally, an internal coordinate dominating $\mathbf{t}(s)$ has only a small influence on $\mathbf{k}(s)$ at that point, and vice versa.

The curvature diagram (Figure 9, with s in $u^{1/2}$ bohr) reveals two phases for the **1a**→**1b** isomerization: phase 1 starts with maximum total curvature near the reactant ($s=-3.5$), decreases smoothly over a long range, and ends at the curvature minimum M1 ($s=2.85$). A short phase 2 follows that is completed at $s=3.8$ with the second curvature maximum. The curvature changes in Figure 9 are small, which is typical of partial cleavage of a multiple bond while a single bond is preserved, as for internal rotation in ethylene. **TS1** is located in the middle of phase 1 and does not play a special role in the transformation of the electronic structure, as seen from the lack of features in the curvature diagram. Phases 1 and 2 correspond to two forms of **1** that can be distinguished by their

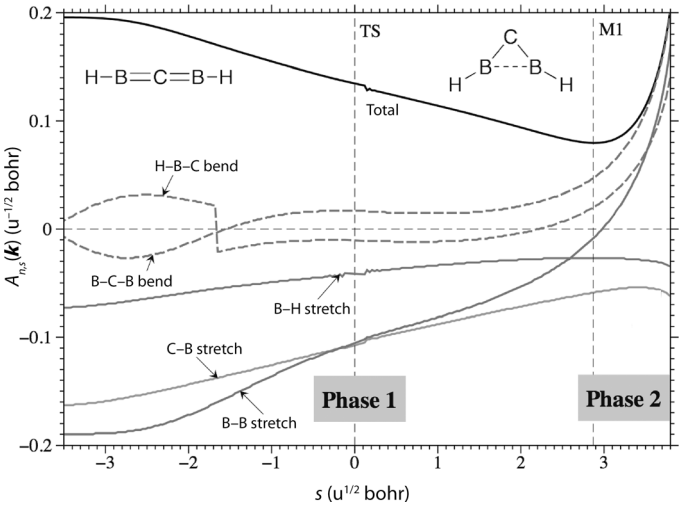

Figure 9. Total curvature and coupling coefficients $A_{n,s}(\mathbf{k};s)$ for each local mode n as a function of arc length s along the $C(BH)_2$ isomerization path, at the MP2/6-31G(d,p) level of theory.

electronic structures.

The local-mode decomposition of the curvature is unusual in that it requires two seemingly redundant parameters, namely, the B–B distance and the B-C-B bending angle, to describe all electronic effects taking place during the **1a**→**1b** isomerization. The B-C-B angle probes electronic reorganization at the carbon atom, for example, rehybridization from sp to sp^2, whereas the B–B distance is necessary to account for charge reorganization in the boron sp-hybridized σ orbitals and the through-space 1,3-boron–boron interactions. At the beginning of the reaction, the negative B-C-B and C–B curvature coupling coefficients in Figure 9 signal resistance to the associated linear bending and bond weakening. Bending requires rehybridization at the C atom, which is opposed by the allenic B-C-B unit. Reflecting exchange repulsion between the two boron atoms, the B–B

distance exhibits the largest $A_{n,s}(\mathbf{k};s)$ coefficient and strongest resistance to bending until the transition state is reached. Only the H-B-C angle is supportive at the early stages of the isomerization.

In phase 1, a critical point in the chemical transformation occurs at $s=-1.62$, where the coupling coefficient for B-C-B bending changes from negative to positive. At this point carbon rehybridization is no longer resistive but supportive, that is, the molecule leaves a distorted allenic form to adopt a bent form with different electronic structure and bonding. Concomitantly, $A_{n,s}(\mathbf{k};s)$ for the resisting B–B mode becomes smaller in size, while the H-B-C angle decreases from 182 to 178° with a corresponding jump in its curvature coupling coefficient.

The transition state for the isomerization does not result from any particular chemical change. As the linear allenic 4π system changes into a bent form with just two π electrons, the C–B bond order decreases, coupled to a smaller weakening of the B–H bond. The collective increase of these and other energy contributions, such as repulsive 1,3 B–B interactions, gives rise to the transition state. Afterwards at M1, the B–B interactions switch from repulsive to attractive, as revealed by the sign change of the corresponding curvature coupling coefficient. This transformation plays the key role in moving from carbon reorganization phase 1 to phase 2, in which the bent form of **1** is finalized. At the final reaction-path point ($s=3.8$), the supportive B–B, B-C-B, and H-B-C curvature coupling coefficients all reach maximum values.

The evolution of NBO charges along the reaction path is shown in Figure 10. Reactant **1a** has an sp-hybridized

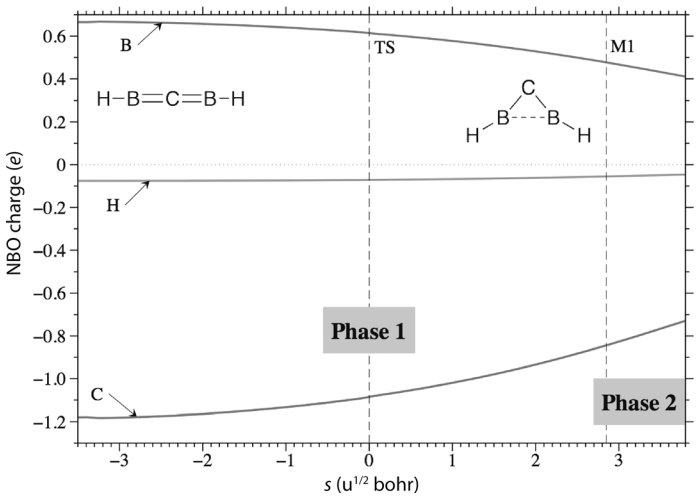

Figure 10. Natural bond orbital (NBO) atomic charges as a function of arc length s along the $C(BH)_2$ isomerization path, at the MP2/6-31G(d,p) level of theory.

carbon with a large negative charge $q(C)=-1.18\,e$, whereas in product **1b** the charge on carbon is only $-0.72\,e$. The change in $q(C)$ is monotonic, starting slowly in the entrance channel and accelerating in phase 2. Overall the carbon atom loses 0.46 electrons, each boron atom gains 0.26 electrons, and the hydrogen atom charges hardly change. As shown in Figure S2 in the Supporting Information, the redistribution of the π electrons along the reaction path follows the same trends. The carbon π_x occupation perpendicular to the plane of bending is 1.22 in **1a** but only 1.05 in **1b**; simultaneously, the π_x occupation of each B atom increases from 0.38 to 0.47. In contrast, the σ charge between the two boron atoms decreases, as reflected by the total boron p_y orbital populations of 1.54 in **1a** and 1.25 in **1b** (Figure S3 in the Supporting Information). In the entrance channel this decrease parallels the reduction of the B–B distance, whereas in phase 2 it levels out. Clearly, there is enough overall charge between the boron atoms to create stabilizing B–B interactions, in line with the B–B bond order of 0.123, but not enough to form a full bond and three-membered ring.

Conclusion

This comprehensive study has produced a number of firm conclusions regarding the $C(BH)_2$ system. Foremost, the linear (**1a**) and bent (**1b**) isomers are energetically degenerate within an uncertainty of ± 0.10 kcal mol^{-1} and are separated by a barrier of only 1.9 kcal mol^{-1}. Quantum tunneling of the heavy-atom framework engenders interconversion between **1a** and **1b** on a timescale much less than 1 s, even at cryogenic temperatures. The bond lengths of the **1a**, **1b**, and TS structures are r_e(B–C) = 1.355, 1.368, 1.358 Å and r_e(B–H) = 1.168, 1.170, 1.169 Å, respectively, as the AE-CCSD(T)/CBS limit is approached, and the corresponding B-C-B bond angles are 180, 90.4, and 125.2°, respectively. The C–B bond length of **1a** is very short, almost 0.1 Å less than the standard value for a covalent C=B double bond. The B–B interatomic distance of 1.946 Å (AE-CCSD(T)/cc-pCVQZ) in **1b** suggests some degree of attractive interaction but still exceeds the prototypical B–B single-bond length by about 0.25 Å. The AIM analysis of **1b** shows that no B–B bond path is present. Careful geometry optimizations did not find an energy minimum for a genuine cyclic form of $C(BH)_2$.

Previous matrix-isolation IR assignments of the $\nu_3(\sigma_u^+)$ and $\nu_4(\sigma_u^+)$ fundamentals of linear $C(BH)_2$ were confirmed by precise matching of band origins and isotopic shifts with our anharmonic FC-CCSD(T)/cc-pVTZ and AE-CCSD(T)/cc-pCVQZ vibrational frequencies. The AE-CCSD(T)/cc-pCVQZ infrared spectrum of the heretofore unobserved bent isomer contains only two fundamentals with substantial intensity, $\nu_7=2715$ cm^{-1} and $\nu_8=1537$ cm^{-1}, both of which are unoccluded and considerably downshifted relative to the corresponding absorptions in the linear form. The ν_7 and ν_8 absorptions of **1b** have only about 40 and 20% of the intensity of their **1a** counterparts, respectively, and thus are inherently more difficult to detect.

Bonding analyses show that **1a** is a classical cumulene HB=C=BH with pairs of three-center two-electron π bonds, whereas **1b** is best characterized as a carbene with little carbone character. Both isomers have a prodigious average C–

B bond-dissociation energy (D_0) of 147 kcal mol^{-1}. Despite its unusual shape and bonding, **1b** has a predominantly closed-shell electronic structure without substantial diradical character. The Laplacian of the electron density around the carbon atom in **1b** does not have a shape typical for lone-pair electrons. The HOMO in the bent isomer facilitates strong C→BH π back-donation that reduces the lone-pair character. The HOMO−1 of **1b** is an in-plane molecular orbital that enhances B–C bonding and yields partial B–B bonding; some σ lone-pair character on carbon is present, but there is significant backside bonding overlap with boron sp hybrids. Analysis of local-mode adiabatic stretching force constants compared to reference compounds gives C–B bond orders of 2.25 and 2.03 in **1a** and **1b**, respectively; the same approach assigns a bond order of 0.12 for the B–B interaction in **1b**.

The URVA analysis describes the **1a**→**1b** isomerization as a chemical process driven by the reorganization of charge at both C and B atoms leading to a bent carbene structure **1b**, which possesses slightly weaker C–B and B–H bonds but gains some extra stabilization through favorable 1,3 B–B interactions. Surprisingly, only small changes in the C–B bond lengths (≈0.013 Å) occur during the **1a**→**1b** isomerization. The curvature of the **1a**→**1b** reaction path reveals two phases for the isomerization: a long phase 1 with smooth curvature decrease over the range $s \in (-3.5, 2.85)$, and a short phase 2 with sharper curvature increase for $s \in (2.85, 3.8)$. A key point in phase 1 occurs at $s = -1.62$, where carbon rehybridization changes from resistive to supportive, as signaled by the coupling coefficient for B-C-B bending. The **1a**→**1b** isomerization starts with a large negative NBO charge of $-1.18\,e$ on carbon; as the transformation proceeds, the C atom loses 0.46 electrons, each B atom gains 0.26 electrons, and the H atom charges hardly change.

Acknowledgements

We are grateful to Chia-Hua Wu for assistance with the vibrational anharmonicity computations. The work in Marburg was supported by the Deutsche Forschungsgemeinschaft. The research at the University of Georgia was supported by the U.S. Department of Energy, Office of Basic Energy Sciences, Combustion Program (grant no. DE-FG02-97ER14748). Assistance with the ACS connection schemes and the URVA calculations by Robert Kalescky and Marek Freindorf are acknowledged. The research at Southern Methodist University was supported by the U.S. National Science Foundation (grant no. CHE 1152357).

[1] a) R. Tonner, F. Öxler, B. Neumüller, W. Petz, G. Frenking, *Angew. Chem.* **2006**, *118*, 8206; *Angew. Chem. Int. Ed.* **2006**, *45*, 8038; b) R. Tonner, G. Frenking, *Angew. Chem.* **2007**, *119*, 8850; *Angew. Chem. Int. Ed.* **2007**, *46*, 8695; c) R. Tonner, G. Frenking, *Chem. Eur. J.* **2008**, *14*, 3260; d) R. Tonner, G. Frenking, *Chem. Eur. J.* **2008**, *14*, 3273; e) G. Frenking, R. Tonner, *Pure Appl. Chem.* **2009**, *81*, 597; f) S. Klein, R. Tonner, G. Frenking, *Chem. Eur. J.* **2010**, *16*, 10160; g) C. Esterhuysen, G. Frenking, *Chem. Eur. J.* **2011**, *17*, 9944.

[2] a) C. A. Dyker, V. Lavallo, B. Donnadieu, G. Bertrand, *Angew. Chem.* **2008**, *120*, 3250; *Angew. Chem. Int. Ed.* **2008**, *47*, 3206; b) A. Fürstner, M. Alcarazo, R. Goddard, C. W. Lehmann, *Angew. Chem.* **2008**, *120*, 3254; *Angew. Chem. Int. Ed.* **2008**, *47*, 3210; c) V. Lavallo, C. A. Dyker, B. Donnadieu, G. Bertrand, *Angew. Chem.* **2008**, *120*, 5491; *Angew. Chem. Int. Ed.* **2008**, *47*, 5411; d) M. Alcarazo, C. W. Lehmann, A. Anoop, W. Thiel, A. Fürstner, *Nat. Chem.* **2009**, *1*, 295; e) M. Melaimi, P. Parameswaran, B. Donnadieu, G. Frenking, G. Bertrand, *Angew. Chem.* **2009**, *121*, 4886; *Angew. Chem. Int. Ed.* **2009**, *48*, 4792; f) I. Fernández, C. A. Dyker, A. DeHope, B. Donnadieu, G. Frenking, G. Bertrand, *J. Am. Chem. Soc.* **2009**, *131*, 11875; g) W. Petz, F. Öxler, B. Neumüller, R. Tonner, G. Frenking, *Eur. J. Inorg. Chem.* **2009**, 4507; h) B. Inés, M. Patil, J. Carreras, R. Goddard, W. Thiel, M. Alcarazo, *Angew. Chem.* **2011**, *123*, 8550; *Angew. Chem. Int. Ed.* **2011**, *50*, 8400.

[3] a) F. Ramirez, N. B. Desai, B. Hansen, N. McKelvie, *J. Am. Chem. Soc.* **1961**, *83*, 3539; b) G. E. Hardy, J. I. Zink, W. C. Kaska, J. C. Baldwin, *J. Am. Chem. Soc.* **1978**, *100*, 8001; c) H. Schmidbaur, *Angew. Chem.* **1983**, *95*, 980; *Angew. Chem. Int. Ed. Engl.* **1983**, *22*, 907; d) W. C. Kaska, *Coord. Chem. Rev.* **1983**, *48*, 1; e) A. W. Johnson, W. C. Kaska, K. A. O. Starzewski, D. A. Dixon, *Ylides and Imines of Phosphorus*, Wiley&Sons, New York, **1993**; f) O. I. Kolodiazhnyi, *Phosphorous Ylides: Chemistry and Application in Organic Synthesis*, Wiley-VCH, Weinheim, **1999**; g) O. I. Kolodiazhnyi, *Tetrahedron* **1996**, *52*, 1855; h) N. D. Jones, R. G. Cavell, *J. Organomet. Chem.* **2005**, *690*, 5485; i) W. Petz, G. Frenking, *Top. Organomet. Chem.* **2010**, *30*, 49.

[4] a) O. Diels, B. Wolf, *Ber. Dtsch. Chem. Ges.* **1906**, *39*, 689; b) A. Ellern, T. Drews, K. Seppelt, *Z. Anorg. Allg. Chem.* **2001**, *627*, 73.

[5] P. Jensen, J. W. C. Johns, *J. Mol. Spectrosc.* **1986**, *118*, 248. The bending potential of C_3O_2 is very shallow and the calculated energy difference between the bent equilibrium structure and the linear form is <0.1 kcal mol^{-1}: J. Koput, *Chem. Phys. Lett.* **2000**, *320*, 237. Carbon suboxide in the solid state adopts a linear geometry, see ref. [4b].

[6] For a quantitative comparison of the acceptor strength of PR_3, CO, and other ligands, see: G. Frenking, K. Wichmann, N. Fröhlich, C. Loschen, M. Lein, J. Frunzke, V. M. Rayón, *Coord. Chem. Rev.* **2003**, *238–239*, 55.

[7] S. Klein, G. Frenking, *Angew. Chem.* **2010**, *122*, 7260; *Angew. Chem. Int. Ed.* **2010**, *49*, 7106.

[8] P. Jerabek, Diploma thesis, Marburg, **2010**.

[9] P. Hassanzadeh, L. Andrews, *J. Am. Chem. Soc.* **1992**, *114*, 9239.

[10] a) J. Čížek, *J. Chem. Phys.* **1966**, *45*, 4256; b) J. Čížek, *Adv. Chem. Phys.* **1969**, *14*, 35; c) J. Čížek, J. Paldus, *Int. J. Quantum Chem.* **1971**, *5*, 359; d) T. D. Crawford, H. F. Schaefer III, *Rev. Comput. Chem.* **2000**, *14*, 33.

[11] a) K. Raghavachari, G. W. Trucks, J. A. Pople, M. Head-Gordon, *Chem. Phys. Lett.* **1989**, *157*, 479; b) J. F. Stanton, *Chem. Phys. Lett.* **1997**, *281*, 130.

[12] a) T. H. Dunning, Jr., *J. Chem. Phys.* **1989**, *90*, 1007; b) D. E. Woon, T. H. Dunning, Jr., *J. Chem. Phys.* **1995**, *103*, 4572; c) A. K. Wilson, T. van Mourik, T. H. Dunning, Jr., *J. Mol. Struc.Theochem.* **1996**, *388*, 339.

[13] a) A. G. Császár, W. D. Allen, H. F. Schaefer III, *J. Chem. Phys.* **1998**, *108*, 9751; b) A. L. L. East, W. D. Allen, *J. Chem. Phys.* **1993**, *99*, 4638; c) J. M. Gonzales, C. Pak, R. S. Cox, W. D. Allen, H. F. Schaefer III, A. G. Császár, G. Tarczay, *Chem. Eur. J.* **2003**, *9*, 2173; d) J. P. Kenny, W. D. Allen, H. F. Schaefer III, *J. Chem. Phys.* **2003**, *118*, 7353; e) M. S. Schuurman, S. R. Muir, W. D. Allen, H. F. Schaefer III, *J. Chem. Phys.* **2004**, *120*, 11586.

[14] a) W. J. Hehre, L. Radom, P. v. R. Schleyer, J. A. Pople, *Ab Initio Molecular Orbital Theory*, Wiley-Interscience, New York, **1986**; b) C. C. J. Roothaan, *Rev. Mod. Phys.* **1951**, *23*, 69; c) A. Szabo, N. S. Ostlund, *Modern Quantum Chemistry*, McGraw-Hill, New York, **1989**.

[15] a) D. Feller, *J. Chem. Phys.* **1993**, *98*, 7059; b) T. Helgaker, W. Klopper, H. Koch, J. Noga, *J. Chem. Phys.* **1997**, *106*, 9639.

[16] C. Møller, M. S. Plesset, *Phys. Rev.* **1934**, *46*, 618.

[17] a) C. Hampel, K. A. Peterson, H. J. Werner, *Chem. Phys. Lett.* **1992**, *190*, 1; b) J. F. Stanton, J. Gauss, J. D. Watts, R. J. Bartlett, *J. Chem.*

Phys. **1991**, *94*, 4334; c) G. D. Purvis, R. J. Bartlett, *J. Chem. Phys.* **1982**, *76*, 1910.
[18] a) Y. J. Bomble, J. F. Stanton, M. Kállay, J. Gauss, *J. Chem. Phys.* **2005**, *123*, 054101; b) M. Kállay, J. Gauss, *J. Chem. Phys.* **2005**, *123*, 214105.
[19] A. C. Simmonett, N. J. Stibrich, B. N. Papas, H. F. Schaefer, W. D. Allen, *J. Phys. Chem. A* **2009**, *113*, 11643.
[20] a) J. F. Stanton, J. Gauss, J. D. Watts, P. G. Szalay, R. J. Bartlett with contributions from A. A. Auer, D. B. Bernholdt, O. Christiansen, M. E. Harding, M. Heckert, O. Heun, C. Huber, D. Jonsson, J. Jusélius, W. J. Lauderdale, T. Metzroth, C. Michauk, D. R. Price, K. Ruud, F. Schiffmann, A. Tajti, M. E. Varner, J. Vázquez and the integral packages: MOLECULE (J. Almlöf and P. R. Taylor), PROPS (P. R. Taylor), and ABACUS (T. Helgaker, H. J. Aa. Jensen, P. Jørgensen, and J. Olsen); b) J. F. Stanton, J. Gauss, J. D. Watts, W. J. Lauderdale, R. J. Bartlett, *Int. J. Quantum Chem.* **1992**, *44*, 879.
[21] CFOUR, J. F. Stanton, J. Gauss, M. E. Harding, P. G. Szalay with contributions from A. A. Auer, R. J. Bartlett, U. Benedikt, C. Berger, D. E. Bernholdt, Y. J. Bomble, L. Cheng, O. Christiansen, M. Heckert, O. Heun, C. Huber, T. C. Jagau, D. Jonsson, J. Jusélius, K. Klein, W. J. Lauderdale, D. A. Matthews, T. Metzroth, D. P. O'Neill, D. R. Price, E. Prochnow, K. Ruud, F. Schiffmann, W. Schwalbach, S. Stopkowicz, A. Tajti, J. Vázquez, F. Wang, and J. D. Watts, and the integral packages MOLECULE (J. Almlöf and P. R. Taylor), PROPS (P. R. Taylor), ABACUS (T. Helgaker, H. J. Aa. Jensen, P. Jørgensen, and J. Olsen), and ECP routines by A. V. Mitin and C. v. Wüllen. For the current version, see http://www.cfour.de.
[22] a) H. J. Werner, P. J. Knowles, R. Lindh, F. R. Manby, M. Schütz, et al. MOLPRO, version 2006.1, a package of ab initio programs. See http://www.molpro.net; b) H.-J. Werner, P. J. Knowles, G. Knizia, F. R. Manby, M. Schütz, et al. MOLPRO, version 2010.1, a package of ab initio programs. See http://www.molpro.net.
[23] M. Kállay, P. R. Surján, *J. Chem. Phys.* **2001**, *115*, 2945.
[24] J. K. G. Watson in *Vibrational Spectra and Structure, Vol. 6* (Ed.: J. R. Durig), Elsevier, Amsterdam, **1977**, p. 1.
[25] D. PapouŠek, M. R. Aliev, *Molecular Vibrational-Rotational Spectra*, Elsevier, Amsterdam, **1982**.
[26] D. A. Clabo, Jr., W. D. Allen, R. B. Remington, Y. Yamaguchi, H. F. Schaefer, *Chem. Phys.* **1988**, *123*, 187.
[27] W. D. Allen, Y. Yamaguchi, A. G. Császár, D. A. Clabo, R. B. Remington, H. F. Schaefer, *Chem. Phys.* **1990**, *145*, 427.
[28] INTDIF is an abstract program written by Wesley D. Allen for *Mathematica* to perform general numerical differentiations to high orders of electronic structure data. See: R. L. DeKock, M. J. McGuire, P. Piecuch, W. D. Allen, H. F. Schaefer, K. Kowalski, S. A. Kucharski, M. Musiał, A. R. Bonner, S. A. Spronk, D. B. Lawson, S. L. Laursen, *J. Phys. Chem. A* **2004**, *108*, 2893.
[29] A. C. Simmonett, H. F. Schaefer, W. D. Allen, *J. Chem. Phys.* **2009**, *130*, 044301.
[30] W. D. Allen, A. G. Császár, V. Szalay, I. M. Mills, *Mol. Phys.* **1996**, *89*, 1213.
[31] W. D. Allen, A. G. Császár, *J. Chem. Phys.* **1993**, *98*, 2983.
[32] INTDER is a general program written by Wesley D. Allen, which performs sundry vibrational analyses and higher order nonlinear transformations among force field representations.
[33] K. Sarka, J. Demaison in *Computational Molecular Spectroscopy* (Eds.: P. Jensen, P. R. Bunker), Wiley, Chichester, **2000**, p. 255.
[34] T. J. Lee, P. R. Taylor, *Int. J. Quantum Chem. Symp.* **1989**, *23*, 199.
[35] C. L. Janssen, I. M. B. Nielsen, *Chem. Phys. Lett.* **1998**, *290*, 423.
[36] H. J. Werner, W. Meyer, *J. Chem. Phys.* **1981**, *74*, 5794.
[37] a) A. D. Becke, *J. Chem. Phys.* **1986**, *84*, 4524; b) J. P. Perdew, *Phys. Rev. B* **1986**, *33*, 8822; c) F. Weigend, R. Ahlrichs, *Phys. Chem. Chem. Phys.* **2005**, *7*, 3297.
[38] P. Pyykkö, M. Atsumi, *Chem. Eur. J.* **2009**, *15*, 12770.
[39] P. Pyykkö, S. Riedel, M. Patzschke, *Chem. Eur. J.* **2005**, *11*, 3511.
[40] HCB has a triplet ($^3\Pi$) electronic ground state. The $^1\Sigma^+$ state is predicted at MP4/6-311G(d,p)//HF/6-31G(d) to be 40.1 kcal mol^{-1} higher in energy than the ground state: B. T. Luke, J. A. Pople, P. v. R. Schleyer, *Chem. Phys. Lett.* **1985**, *122*, 19.
[41] a) I. L. Alberts, H. F. Schaefer III, *Chem. Phys. Lett.* **1990**, *165*, 250; b) J. Poater, M. Solá, C. Viñas, F. Teixidor, *Chem. Eur. J.* **2013**, *19*, 4169.
[42] P. Pyykkö, M. Atsumi, *Chem. Eur. J.* **2009**, *15*, 186.
[43] a) A. Szabó, A. Kovács, G. Frenking, *Z. Allg. Anorg. Chem.* **2005**, *63*, 1803; b) M. Lein, A. Szabó, A. Kovács, G. Frenking, *Faraday Discuss.* **2003**, *124*, 365.
[44] C. E. Moore, *Atomic Energy Levels*; NSDRS-NBS 35; U. S. National Bureau of Standards, Washington, DC **1971**.
[45] K. P. Huber, G. Herzberg, *Molecular Spectra and Molecular Structure IV. Constants of Diatomic Molecules*, Van Nostrand-Reinhold, New York, **1979**.
[46] E. Miliordos, A. Mavridis, *J. Chem. Phys.* **2008**, *128*, 144308.
[47] R. P. Bell, *Tunnel Effect in Chemistry*, Chapman and Hall, London, New York, **1980**.
[48] P. R. Schreiner, H. P. Reisenauer, F. C. Pickard IV, A. C. Simmonett, W. D. Allen, E. Mátyus, A. G. Császár, *Nature* **2008**, *453*, 906.
[49] D. Gerbig, H. P. Reisenauer, C.-H. Wu, D. Ley, W. D. Allen, P. R. Schreiner, *J. Am. Chem. Soc.* **2010**, *132*, 7273.
[50] P. R. Schreiner, H. P. Reisenauer, D. Ley, D. Gerbig, C.-H. Wu, W. D. Allen, *Science* **2011**, *332*, 1300.
[51] P. Hassanzadeh, Y. Hannachi, L. Andrews, *J. Phys. Chem.* **1993**, *97*, 6418.
[52] R. F. W. Bader, *Atoms in Molecules: A Quantum Theory*, Clarendon Press, Oxford, **1990**.
[53] Note that the absence of a bond path does not mean that there is no chemical bond between two atoms. For a recent example, see: M. Mousavi, G. Frenking, *J. Organomet. Chem.* asap. DOI: http://dx.doi.org/10.1016/j.jorganchem.2013.03.047.
[54] In a normal carbene CR_2, the σ orbital at carbon is occupied yielding a lone-pair MO, while the p(π) orbital at carbon is empty. A "reversed" carbene has opposite orbital occupation.
[55] The latter perspective has been suggested by R. Hoffmann in a study where the dimers of $C(BH)_2$ have been investigated with quantum chemical methods: A. Yu. Rogachev, P. Jerabek, S. Klein, G. Frenking, R. Hoffmann, *Theor. Chem. Acc.* **2012**, *131*, 1149.
[56] R. Tonner, G. Heydenrych, G. Frenking, *ChemPhysChem* **2008**, *9*, 1474.
[57] W. Zou, R. Kalescky, E. Kraka, D. Cremer, *J. Chem. Phys.* **2012**, *137*, 084108.
[58] R. Kalescky, W. Zhou, E. Kraka, D. Cremer, *Chem. Phys. Lett.* **2012**, *554*, 243.
[59] Z. Konkoli, D. Cremer, *Int. J. Quantum Chem.* **1998**, *67*, 1.
[60] Z. Konkoli, D. Cremer, *Int. J. Quantum Chem.* **1998**, *67*, 29.
[61] D. Cremer, E. Kraka, *Curr. Org. Chem.* **2010**, *14*, 1524.
[62] E. Kraka, A. J. Larsson, D. Cremer in *Computational Spectroscopy: Methods, Experiments and Applications* (Ed.: J. Grunenberg), Wiley-VCH, Weinheim, **2010**, pp. 105–149.
[63] M. Freindorf, E. Kraka, D. Cremer, *Int. J. Quantum Chem.* **2012**, *112*, 3174.
[64] E. Kraka, D. Cremer, *ChemPhysChem* **2009**, *10*, 686.
[65] E. Kraka, *WIREs Comput. Mol. Sci.* **2011**, *1*, 531.
[66] E. Kraka, D. Cremer, *Acc. Chem. Res.* **2010**, *43*, 591.

Received: June 7, 2013
Published online: October 7, 2013

